*Desalination and Water Treatment*
www.deswater.com
doi: 10.5004/dwt.2020.24938

178 (2020) 41–52
February

# Evolutionary prediction of multiple vertical buoyant jets in stationary ambient water

Xiaohui Yan*, Abdolmajid Mohammadian

*Department of Civil Engineering, University of Ottawa, 161 Louis Pasteur, Ottawa Ontario, K1N6N5, Canada, emails: clarkyanxh@gmail.com (X. Yan), majid.mohammadian@uottawa.ca (A. Mohammadian)*

Received 6 April 2019; Accepted 21 September 2019

**ABSTRACT**

The variables describing the merging and mixing properties of multiple vertical buoyant jets in stationary ambient water have not been generally formulated and reported. This work develops new evolutionary-based models to predict such variables, including for the non-dimensional vertical displacement of the merging point ($y_m/D$), the non-dimensional centerline concentration ($C_m/C_0$) where the jets start merging, the non-dimensional vertical displacement of the well-mixed location ($y_w/D$), and the non-dimensional concentration where the jets are well mixed ($C_w/C_0$). These parameters are crucial in the design of outfall systems and for environmental impact assessments. A fully three-dimensional (3D) computational fluid dynamics model that solves the Navier–Stokes equations and uses the re-normalisation group (RNG) $k$-ε turbulence closure is validated against the available experimental data. The validated numerical model is further utilized to carry out additional computations for 100 different cases to enrich the data sets. The data are employed to develop and evaluate the evolutionary-based models, and the model networks are optimized using multigene genetic programming. The proposed models can serve to compute the mentioned jet characteristic variables as a function of non-dimensional port spacing (Sp) and jet densimetric Froude number (Fr). Partial derivative sensitivity analysis is also conducted to assess how the varying input variables affect the jet characteristic parameters. An uncertainty analysis is also performed for the proposed models. The proposed explicit equations and codes facilitate easy estimation of the merging and mixing properties of vertical buoyant jets discharged from multiport diffusers.

*Keywords:* Artificial intelligence; Computational fluid dynamics; Mixing properties; Multigene genetic programming; Multiple jets; Partial derivative sensitivity analysis

## 1. Introduction

Wastewater effluents that have a lower density than the ambient water are often discharged through multiport diffusers [1–4]. Such jets are known as multiple vertical buoyant jets when they are discharged vertically into water bodies. When a buoyant jet is discharged into ambient water with sufficient clearance from any boundary or other jets, a shear layer is formed, and the ambient fluid is entrained into the jet due to the shear stresses and thus the jet is diluted [5]. For multiple jets, individual jets may come into contact with neighboring jets, and thus the dilution is restricted, reducing the dilution efficiency (Fig. 1). In outfall or diffuser designs, it is better to avoid jet interactions in order to improve the degree of dilution and to ensure that high dilution takes place in a limited mixing zone [6]. However, this is usually impossible in practice due to the huge volumes of wastewater being discharged and the limitation of project budgets [3,7]. Therefore, it is necessary to better understand the flow and mixing processes of multiple vertical buoyant jets in order to ensure the proper disposal of the wastewater

* Corresponding author.

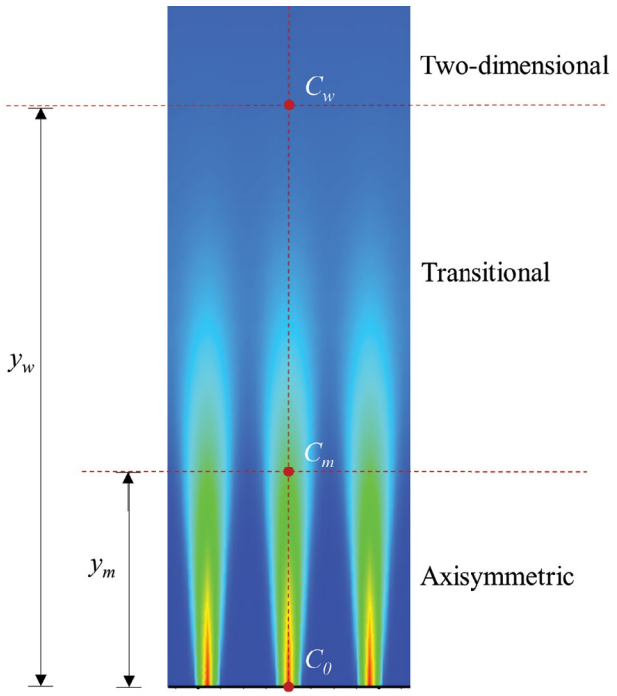


Fig. 1. Schematic diagram of multiple vertical buoyant jets.

and avoid potential adverse effects on the environment and ecology [8–13].

Wastewater effluents can be investigated using various methods, with physical or laboratory studies currently being the most popular research methods. Recent experimental works have mainly involved investigations on single jets; examples include an isothermal jet issuing horizontally from a round nozzle into a shallow layer of water [14], negatively buoyant surface discharge in an ambient current under a variety of conditions [15], negatively buoyant discharges in which the boundary influences were eliminated [16], and 30° and 45° inclined dense jets in shallow coastal waters [17]. A limited number of experimental works have involved studies on jets discharged from multiple diffusers, such as a comprehensive laboratory study on wastewater diffusers with multiport rosettes [4], experiments on multiport diffusers for dense effluents into stationary receiving waters [1], and experimental investigation on the behavior of multiple vertical buoyant jets discharged into stagnant ambient water [3]. Despite the scale effects, these methods are quite accurate and reliable; however, they are usually quite expensive and time-consuming, restricting their wider application in practical engineering problems.

In addition to physical or experimental methods, many researchers have developed theoretical or numerical models to study the mixing properties of wastewater effluent jets. Integral models such as the CORMIX3 expert system [18,19], the CorSuf system [20], and the Modified CorJet system [12] are widely used in both academic and practical applications. Recent advances in computational techniques and resources have provided a new avenue of modeling wastewater effluent jets by solving fully three-dimensional (3D) Navier–Stokes equations. These 3D computational fluid dynamics (CFD) models have been developed and applied for turbulent wall jets in stationary ambient water [21–23], 45° inclined dense jets [13], and vertical buoyant jets subjected to lateral confinement [5]. These studies have demonstrated well that a 3D CFD model can provide satisfactory results for the mixing properties of a wastewater jet. However, CFD modeling is still very time-consuming and requires measurements for validation, so its wider application in practical engineering problems is also restricted.

In the past several years, genetic programming (GP), a well recognized artificial intelligence (AI) algorithm, has been successfully utilized in many engineering applications and has proven to be more advanced than conventional methods [24–27]. The present study focuses on the multigene genetic programming (MGGP) technique, which is a recent advancement of GP [28–30]. Garg et al. [31] employed an MGGP technique for the simulation of soil water retention curves. They also conducted parametric sensitivity analyses and found explicit equations that can effectively describe the nonlinear relationship between the degree of saturation, the suction, and the net stress of three different soils. Their study demonstrated that MGGP can be a powerful tool to provide detailed numerical information on soil water energetic states. Kaydani et al. [32] utilized the MGGP technique to perform permeability estimations in heterogeneous oil reservoirs, and their results showed the superiority of the MGGP model in predicting the permeability of porous media as compared with the ANNs, ANFIS, and GP techniques, especially in terms of the capability of generating compact models and not suffering from structural dependency. Safari and Mehr [29] used MGGP to model the sediment transport in sewers for conditions of non-deposition with a bed deposit. Their study indicated the higher efficiency of the technique in comparison with conventional regression models. Mehr and Nourani [33] proposed a new rainfall-runoff model that integrated a season algorithm with MGGP, and the results implied that MGGP was better than monolithic GP in identifying the underlying structure of the rainfall-runoff process at Haldizen Catchment, Trabzon, Turkey. Yan and Mohammadian [34] applied MGGP to predict the initial dilution of laterally confined vertical buoyant jets, Yan and Mohmmadian [35] used MGGP to model inclined dense jets discharged from multiport diffusers, and both studies demonstrated that MGGP was better than traditional methods.

To the authors' knowledge, MGGP has never been applied to predict the variables that describe the mixing properties of multiple vertical buoyant jets in stationary ambient water. In addition, some challenges remain in terms of design improvement considerations for multiple vertical buoyant jets because the mixing and dilution properties have not been adequately understood. The vertical displacement of the merging point and the centerline concentration where the jets start merging (the transition between the axisymmetric zone and the transitional zone) are the primary parameters describing the merging properties of jets discharged from multiport diffusers, and thus are important considerations in outfall designs and environmental impact assessments. Above the location that the merging process is completed (the transition between the transitional zone and two-dimensional zone, hereafter referred to as

the "well-mixed location"), the jets follow the behavior of a large two-dimensional (2D) jet, and thus additional properties can be predicted by using the well-established expertise and knowledge of 2D single jets. Therefore, the vertical displacement of the well-mixed location and the concentration where the jets are well mixed are also very important characteristic variables.

Therefore, the objectives of this work are threefold: (1) to verify whether the MGGP technique can correlate the important characteristic variables of multiple jets with the flow input values; (2) to develop and present explicit equations for calculating the characteristic variables using MGGP; and (3) to assess how varying input parameters can affect the crucial variables.

## 2. Methodology

### 2.1. Analysis of multiple jets

Previous studies on single jets [36–38] have pointed out that the flow and mixing properties of the jets are primarily dominated by the jet densimetric Froude number, Fr. Fr denotes the ratio of inertia to buoyancy force, and is defined as:

$$\mathrm{Fr} = \frac{U_0}{\sqrt{g'D}} \tag{1}$$

with

$$g' = g\frac{\rho_a - \rho_j}{\rho_a} \tag{2}$$

where $U_0$ is the initial velocity, $D$ is the diameter of the discharge port, $g$ is the gravitational acceleration, g' is the modified gravitational acceleration, $\rho_a$ is the ambient density, and $\rho_j$ is the jet's initial density.

This study focuses on multiple vertical buoyant jets in stationary ambient water. For multiple jets, the effect of port spacing should also be considered. Therefore, the non-dimensional vertical displacement of the merging point ($y_m/D$), the non-dimensional centerline concentration ($C_m/C_0$) where the jets start merging, the non-dimensional vertical displacement of the well-mixed location ($y_w/D$), and the non-dimensional concentration where the jets are well mixed ($C_w/C_0$) can be written as functions of Fr and the non-dimensional port spacing Sp (distance between two neighboring ports divided by the port diameter) as:

$$\frac{y_m}{D} = f\left(\mathrm{Fr},\mathrm{Sp}\right) \tag{3}$$

$$\frac{C_m}{C_0} = f\left(\mathrm{Fr},\mathrm{Sp}\right) \tag{4}$$

$$\frac{y_w}{D} = f\left(\mathrm{Fr},\mathrm{Sp}\right) \tag{5}$$

$$\frac{C_w}{C_0} = f\left(\mathrm{Fr},\mathrm{Sp}\right) \tag{6}$$

### 2.2. CFD modeling

The governing equations for mass and momentum for an incompressible multiphase fluid can be expressed as [38]:

$$\nabla \times U = 0 \tag{7}$$

$$\frac{\partial \rho U}{\partial t} + \nabla\left(\rho \mathrm{UU}\right) = -\nabla\left(p_{\mathrm{rgh}}\right) - \mathrm{gh}\nabla\rho + \nabla\left(\rho T\right) \tag{8}$$

with:

$$\rho = \alpha_1\rho_1 + \alpha_2\rho_2 = \alpha_1\rho_1 + \left(1-\alpha_1\right)\rho_2 \tag{9}$$

$$T = -\frac{2}{3}\bar{\mu}_{\mathrm{eff}}\nabla \mathrm{UI} + \bar{\mu}_{\mathrm{eff}}\nabla U + \bar{\mu}_{\mathrm{eff}}\left(\nabla U\right)^T \tag{10}$$

$$\bar{\mu}_{\mathrm{eff}} = \alpha_1\left(\mu_{\mathrm{eff}}\right)_1 + \alpha_2\left(\mu_{\mathrm{eff}}\right)_2 \tag{11}$$

$$\left(\mu_{\mathrm{eff}}\right)_i = \left(\mu + \mu_t\right)_i \tag{12}$$

where $t$ is time, $U$ is velocity, $\rho$ is density, $p$ represents pressure where $\nabla(p_{\mathrm{rgh}})$ and $\mathrm{gh}\nabla\rho$ are obtained by using $P = p_{\mathrm{rgh}} + \rho gh$, $g$ is gravitational acceleration, $T$ is the stress–strain tensor, $\alpha$ is volume fraction, with subscript $i$ denoting either fluid 1 or 2, $I$ is the identity tensor, $T$ denotes the transpose operation, $\mu_{\mathrm{eff}}$ is the effective viscosity, $\mu$ is dynamic viscosity, and $\mu_t$ is turbulent viscosity.

The alpha diffusion equation is given as:

$$\frac{\partial \alpha_1}{\partial t} + \nabla\left(U\alpha_1\right) = \nabla\left(\left(D_{\mathrm{ab}} + \frac{\nu_t}{S_C}\right)\nabla\alpha_1\right) \tag{13}$$

where $D_{\mathrm{ab}}$ is the molecular diffusivity, $\nu_t$ is the turbulent eddy viscosity, and $S_C$ is the turbulent Schmidt number.

The re-normalisation group (RNG) $k$-$\varepsilon$ turbulence model can be expressed as:

$$\frac{\partial \rho k}{\partial t} + \nabla\left(\rho U k\right) - \nabla\left[\alpha_k\mu_{\mathrm{eff}}\nabla k\right] = G - \rho\varepsilon + S_k \tag{14}$$

$$\frac{\partial \rho \varepsilon}{\partial t} + \nabla\left(\rho U \varepsilon\right) - \nabla\left[\alpha_\varepsilon\mu_{\mathrm{eff}}\nabla\varepsilon\right] = c_{1\varepsilon}G\frac{\varepsilon}{k} - c_{2\varepsilon}\rho\frac{\varepsilon^2}{k} - R_\varepsilon + S_\varepsilon \tag{15}$$

where $k$ is the turbulent kinetic energy, $\varepsilon$ is the turbulent energy dissipation rate, $\alpha_k$ and $\alpha_\varepsilon$ are the inverse effective Prandtl numbers for $k$ and $\varepsilon$, respectively, $\mu_{\mathrm{eff}}$ is the effective viscosity, $G$ is the production of turbulence due to shear, $S_k$ and $S_\varepsilon$ are source terms, and $c_{1\varepsilon}$ and $c_{2\varepsilon}$ are model constants equal to 1.44 and 1.92, respectively.

The term $R_\varepsilon$ is given by:

$$R_\varepsilon = \frac{C_\mu\rho\eta^3\left(1-\frac{\eta}{\eta_0}\right)}{1+\beta\eta^2}\frac{\varepsilon^2}{k} \tag{16}$$

where $C_\mu = 0.0845$, $\eta = S_k/\varepsilon$, $\eta_0 = 4.38$, and $\beta = 0.012$.

The effective viscosity is calculated by the differential equation:

$$d\left(\frac{\rho^2 k}{\sqrt{\varepsilon\mu}}\right) = 1.72\frac{\hat{\nu}}{\sqrt{\hat{\nu}^3 - 1 + C_\nu}}d\hat{\nu} \tag{17}$$

where $\hat{\nu} = \mu_{eff}/\mu$ and $C_\nu \approx 100$.

### 2.3. Multigene genetic programming

As mentioned earlier, MGGP is a recent extension of GP. Each gene of a multigene individual is a traditional GP tree that can capture nonlinear behavior. The genes are linearly combined, and their weights are determined using the ordinary least squares approach. For instance, Fig. 2 shows a sample MGGP chromosome. The mathematical model that the chromosome represents is:

$$y = \alpha\left[x_1\cos\left(0.5x_2\right) + \tanh\left(-x_2\right)\right] + \beta\left[1.4\exp\left(x_1^{x_2}\right) - \log\left(x_2\right)\right] + \gamma \tag{18}$$

where $x_1$ and $x_2$ are the input variables, $\alpha$ and $\beta$ are the weights of the genes, and $\gamma$ is the bias term. The chromosome has two genes, which are traditional GP trees that have nonlinear terms. The individual mathematical models that the two trees represent are linearly combined using the weights and the bias term, which are solved using the classical least squares method during the process of model training. Therefore, MGGP combines the best properties of the traditional GP and linear least squares parameter estimation techniques, and allows for multiple genes. Therefore, it can develop models more effectively and accurately than the standard GP. The detailed theory, formulations, and modeling procedures have been well documented elsewhere in the literature [28–30].

### 2.4. Procedure

The experimental data available in the literature are very rare and do not include all aspects of the merging and mixing properties of multiple vertical buoyant jets in stationary ambient water. Therefore, numerical simulations were conducted in this work to enrich the data sets, and the governing and alpha diffusion equations presented in this paper were solved using the finite volume method using a transient solver called "twoLiquidMixingFoam" within the OpenFOAM (Open-source Field Operation and Manipulation) framework. The solver has been widely employed and validated in previous studies [13]. The RNG $k$-ε model, which is a modified version of the standard $k$-ε, was utilized for turbulence modeling. While various solvers are available in the literature, [5,21–23], as well as various turbulence models (e.g., large-eddy simulation, detached-eddy simulation, and realizable k-ε), preparatory studies have shown that the performance of the current simpler solver and turbulence model is satisfactory. The experiment by Lyu et al. [3] was simulated using the numerical model, and the validated numerical model was utilized to carry out additional simulations for 100 cases with different Sp (ranging from 1 to 10 with an interval of 1) and Fr (ranging from 4.5 to 13.5 with an interval of 1) values, which covered the typical data ranges for practical applications, in order to enrich the data sets. A better model can be expected with the utilization of purely experimental data sets, but it is common and practical to use a validated numerical model to enrich data sets when observational data sets are not adequate [39]. The four jet characteristic parameters, namely, $y_m/D$, $C_m/C_0$, $y_w/D$, and $C_w/C_0$, for each case were calculated from the obtained results.

The data were divided into two groups: 80% of the data were randomly selected for use as a training data set, and the remaining were utilized as a testing (unseen) data set, which was the same setup as in Bashiri et al. [40]. The MGGP training and testing were then conducted using the open-source MATLAB code GPTIPS2 [30]. The population size

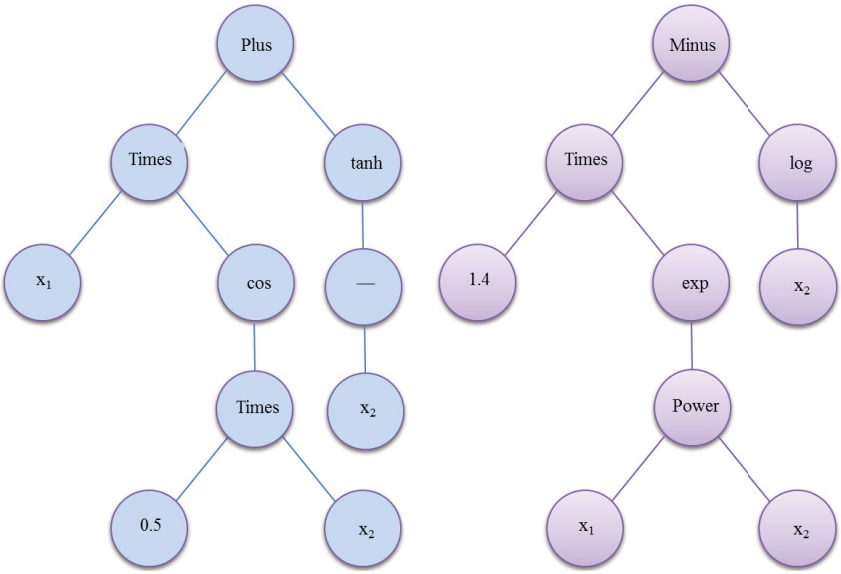


Fig. 2. An example of an MGGP chromosome.

was set at 250, and the maximum generation was set at 1,000. The tournament size was set at 20, and the probability of the Pareto tournament was set at 0.3. The elite fraction was set at 0.3, with approximately 30% of the models being copied from a parent generation to the child generation. The crossover and mutation probabilities were set at 0.84 and 0.14, respectively. The function set contained the most commonly used operators, including 'times', 'minus', 'plus', 'rdivide', 'square', 'sin', 'cos', 'exp', 'mult3', 'add3', 'sqrt', 'cube', 'power', 'negexp', 'neg', 'abs', and 'log'. Based on the evolutionary predictions, the model performance was evaluated. Finally, the variation trends of the parameters with the input variables were analyzed by utilizing the evolved model.

## 3. Results and discussion

### 3.1. Validation of the CFD model

In the experiment by Lyu et al. [3] and in the present CFD simulations for model validation, the nozzles had a diameter of 0.003 m, the port spacing was 0.015 m, the density difference between the jet and the ambient water was 2.297 kg/m$^3$, the initial velocity was 0.111 m/s, and the densimetric Froude number was about 13.5. The diffuser model in the experiment had 24 possible holes for the nozzles, and these nozzles were assumed to be part of an infinite array of nozzles. As shown in Fig. 1, the current simulations, including both the validation case and the additional cases, only incorporated three nozzles, and set the front and back patches as symmetric. The boundary condition at the nozzle surfaces was set as the velocity inlet, and the inlet-outlet boundary condition was used for the top patch. When there is no backward flow, the boundary condition becomes the zero-gradient open boundary condition, and when there is backward flow, the boundary condition automatically becomes a fixed-value boundary condition. No-slip wall boundary conditions were assigned to the walls, and a structured mesh with finer grids closer to the jets was used. The simulated domain was 0.505 m in the transverse direction and 0.7 m in the vertical direction. The dimension in the direction passing through the jet centers varied with the port spacing. PIMPLE algorithms were used for coupling the pressure and momentum. The temporal terms were discretized using the Euler scheme; the gradient terms, velocity divergence terms, and viscous stresses tensor terms were discretized using the Gauss linear scheme; and the Laplacian terms were discretized using the corrected Gauss linear scheme. The maximum Courant number was set as 0.5. A default value of 0.05 s was assigned to the time step, and the model automatically adjusted the time step based on the numerical stability criteria. The end time for the simulations was set as 90 s, which was sufficiently long for the present cases. The number of computational cells was 910,800, and the sensitivity simulations showed that the uncertainty induced by the grid resolution was well below 2%.

The measured and simulated velocity profiles at various locations are presented in Fig. 3. In this figure, the local axial velocity, $U$, is normalized by the local centerline velocity, $U_c$, and the span-wise displacement from the jet center, $x$, is normalized by the vertical displacement from the jet inlet, $y$. The mean bias errors (MBEs), mean absolute errors (MAEs), root mean square errors (RMSEs), and R-squared values ($R^2$s) were calculated and are indicated on the plots.

As can be seen in the plots, the simulated velocity profiles are very close to the measured ones. The average MBE value was –0.014, indicating that the model slightly underestimated the local jet velocity. The average MAE and RMSE values were 0.020 and 0.024, respectively. These values of error indication are quite low, indicating that the modeled results matched the experimental data very well. The smallest $R^2$ value was 0.997, which was very high, again confirming that the model can accurately predict the flow properties of multiple vertical buoyant jets in stationary ambient water. Therefore, the numerical model was used further to carry out additional simulations for 100 different cases in order to enrich the data sets. The jets merged almost immediately when the port spacing was very close (Sp = 1 and 2), and so the data for these cases were not used for further analyses for $y_m$ and $C_m$. Similarly, the jets did not completely mix with each other within the study domain when the port spacing was very far (Sp = 10), and so these data were not included in further analyses for $y_w$ and $C_w$. The final data sets are shown in Fig. 4.

### 3.2. MGGP predictions

The best evolutionary equations obtained by using the MGGP technique for the four jet characteristic variables are summarized in Table 1. Some simpler models were also obtained; however, the simpler models provided lower accuracy without reducing the computational cost, and so they are not discussed further herein.

To compare the data and evolutionary predictions, scatter plots for the four variables, namely $y_m/D$, $C_m/C_0$, $Y_w/D$, and $C_w/C_0$, were made and are presented in Fig. 5. These plots show that almost all the scatter points are very close to the identity line. To obtain a quantitative measure of the difference between the data and predictions, the statistics and the results of the error analysis were calculated and are summarized in Table 2. In addition to MBE, MAE, RMSE, and $R^2$, some additional error measures, including the mean absolute percentage errors (MAPEs) and normalized root-mean-squared errors (NRMSEs), are also presented in order to comprehensively evaluate the prediction performance.

The MGGP model predicted $y_m/D$ very well, as the scatter points shown in Fig. 5a is very close to the identity line. The MBE value was 0.0066, indicating that the MGGP model tended to slightly overestimate the merging locations. The MAE and RMSE values were 0.0563 and 0.0759, respectively, so the error magnitude was about 0.07. The MAPE and NRMSE values were 0.6474% and 0.4083%, respectively, indicating that the error in MGGP prediction for $y_m/D$ was about 0.5%. The $R^2$ value was almost 1, demonstrating that the evolved model predicted the data variation trends almost perfectly.

The evolutionary predictions for $C_m/C_0$ were also very accurate. The MBE value was –0.0001, which is very close to zero, indicating that the model provided a good prediction of the mean jet properties. The MAE and RMSE values were 0.0016 and 0.0024, respectively, so the error magnitude was about 0.002. The MAPE and NRMSE values were 0.5191% and 0.5568%, respectively, indicating that the error in MGGP

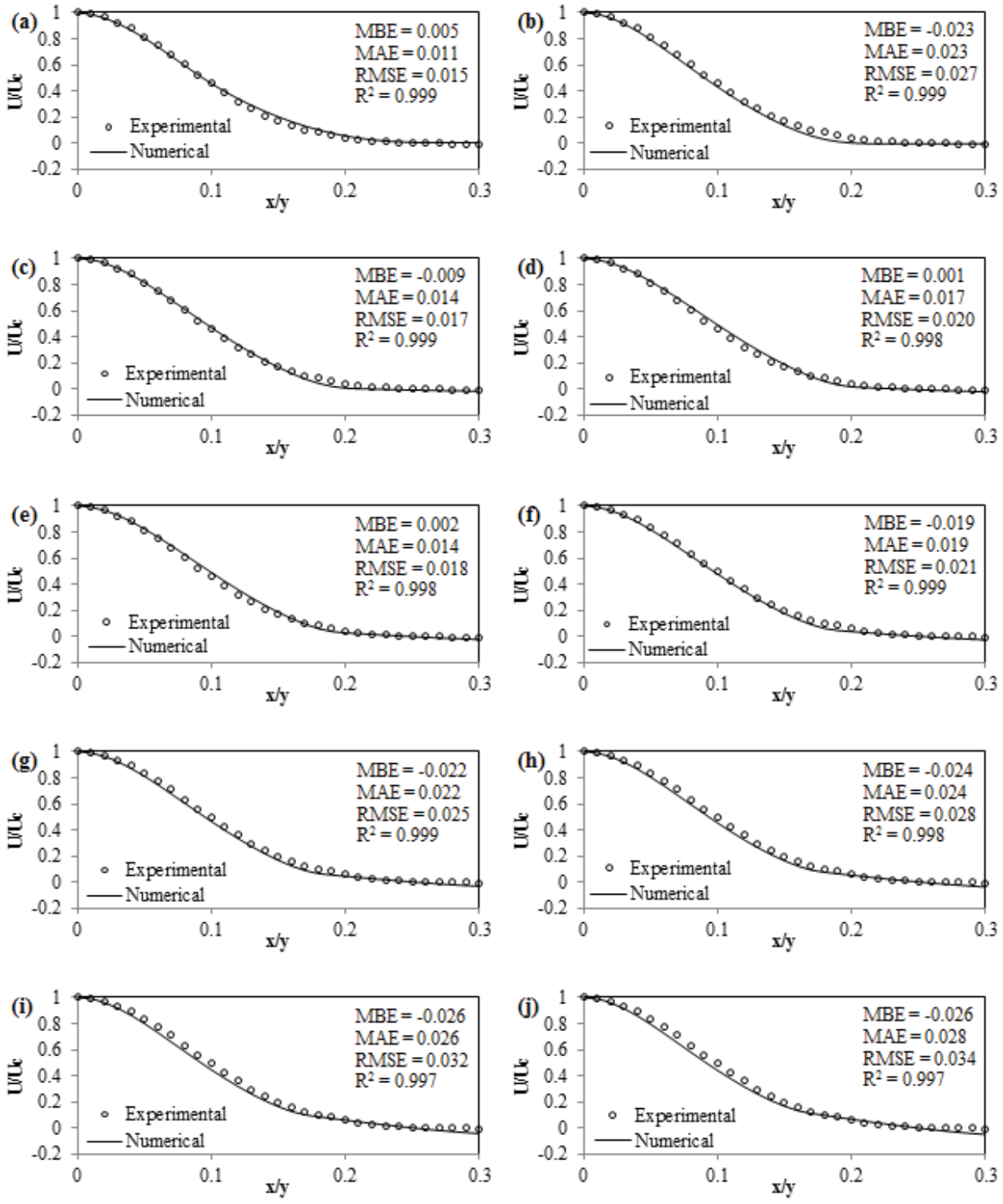


Fig. 3. Comparison of experimental and numerical results of velocity profiles: (a) $y$ = 0.03 m; (b) $y$ = 0.06 m; (c) $y$ = 0.09 m; (d) $y$ = 0.12 m; (e) $y$ = 0.15 m; (f) $y$ = 0.18 m; (g) $y$ = 0.21 m; (h) $y$ = 0.24 m; (i) $y$ = 0.27 m; (j) $y$ = 0.30 m.

prediction for $C_m/C_0$ was about 0.5%, which is close to the prediction accuracy for $y_m/D$. The relative error indicator, $R^2$, was 0.9999, which is very close to 1. The absolute error measures were very low and the relative error measure was quite high, so the results demonstrated the capability of the evolved model to accurately predict $C_m/C_0$ for multiple vertical buoyant jets in stationary ambient water.

The evolved model performed rather worse for $y_w/D$ than for $y_m/D$. The MBE value was 0.0660, implying that the model tended to overestimate the well-mixed locations.

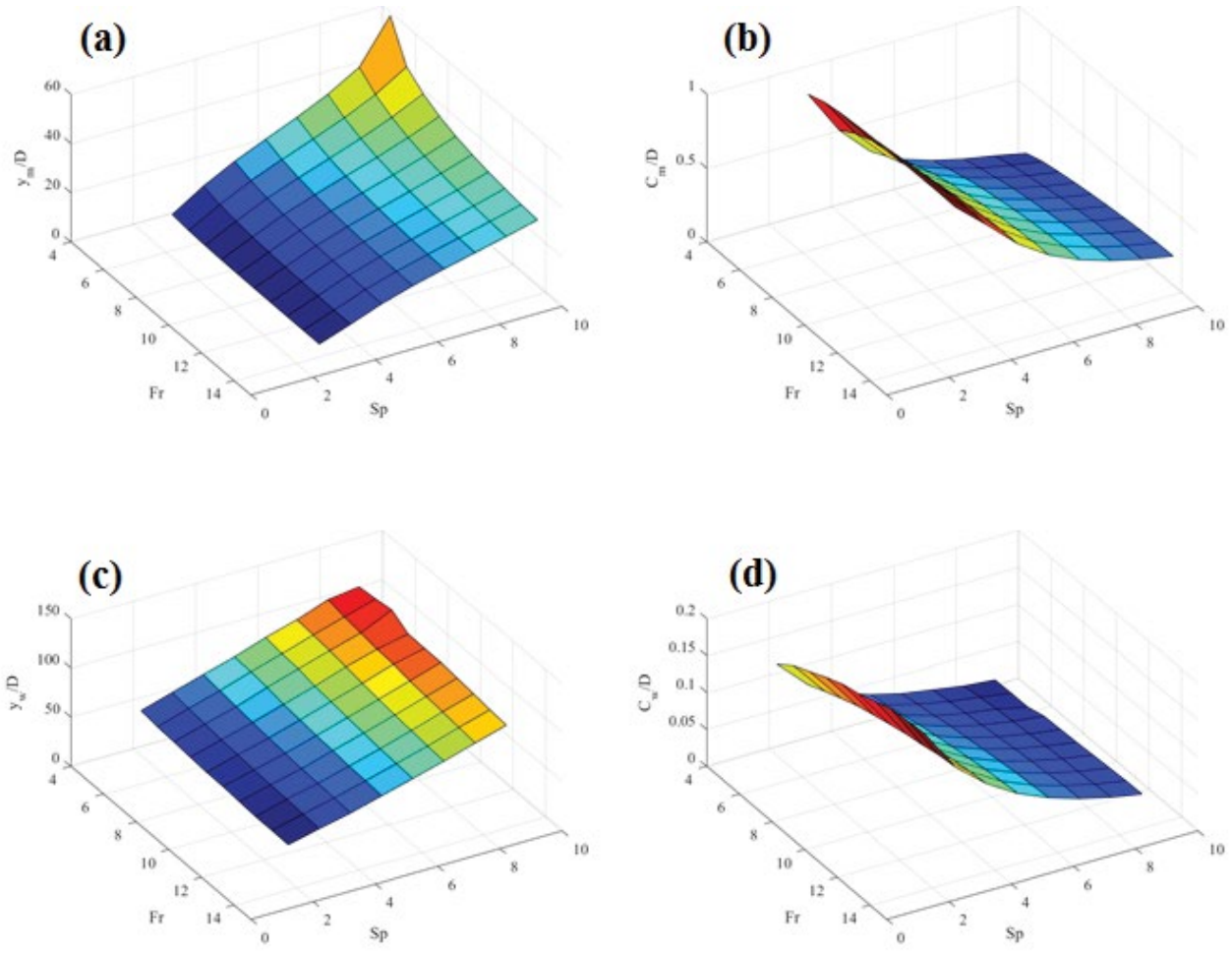


Fig. 4. 3D plots of data sets: (a) $y_m/D$; (b) $C_m/C_0$; (c) $y_w/D$; and (d) $C_w/C_0$.

Table 1
MGGP-based equations for the jet characteristic variables

| Variable | Equation |
|---|---|
| $y_m/D$ | $12Sp + 0.549Fr - 5.75\cos(Sp^{0.5}) + 60\sin(Sp^{0.5}) + 1.41 \times 10^{-4}\exp(Sp^3/Fr^3) - 5.75\log(Fr) + (0.54Sp^2)/Fr - (1.32Sp^3)/Fr^3 + (5.75Sp)/Fr - (4.93Fr)/Sp^2 + 52.3Fr^{(1/Sp^2)} + 1.25\exp(Sp - Fr)^{0.5} - (0.418Sp)/(Fr^2\cos(Fr)\log(Fr)) - 151$ |
| $C_m/C_0$ | $14.8\exp(\exp(\exp(-Sp))) - 0.0108\sin(Sp) + (1.08 \times 10^{-19}(8.93 \times 10^{15}\cos(Fr) + 8.93 \times 10^{15}SpFr^2 + 8.93 \times 10^{15}Fr^2))/Fr^{0.25} + 1.42\sin(\sin(Sp))\exp(-Fr) - 0.0103SpFr - (136\exp(-Sp))/Sp - 0.00299Fr^2 + 0.447Fr^{0.5} + (64.2\exp(-Sp))/(SpFr^{0.25}) - (3.44Spcos(Sp - Fr)\exp(-Sp))/Fr^2 - 40.8$ |
| $y_w/D$ | $5.4Sp - 0.529Fr + 0.251\sin(3.14SpFr) + 0.669\cos(Fr^4) + 0.462\cos(Sp^2/Fr) + 1655\exp(-5Sp) + 0.291\sin(Sp^{Sp}) - (0.251Sp^2)/Fr^3 - (0.0207Sp^9)/Fr^9 + (12.2Sp)/Fr - 8 \times 10^{-4}SpFr^2 + 0.291Sp^2 - 8 \times 10^{-4}Sp^4 - 0.77Fr^{0.5} + 32$ |
| $C_w/C_0$ | $0.0116Fr - 0.15\sin(\log(Sp)) + 1.2 \times 10^{-5}\text{abs}(Sp)^3\text{abs}(Fr) - (0.222\log(Fr)^2)/Fr(Sp) - 5.84 \times 10^{-5}Sp^3 + 0.0314(2.6Sp^2Fr)^{\exp(-*Sp)} + 0.001Fr\exp(-Sp)\cos(Fr) - 0.00102SpFr\log(Sp) - 5.94 \times 10^{-5}Fr^2\log(SpFr)\log(Fr) + 1.47 \times 10^{-4}Fr^2\log(Sp)\log(Fr) + 0.147$ |

The MAE and RMSE values were 0.4845 and 0.7325, respectively, so the error magnitude was about 0.6. The error magnitude was about 10 times that for $y_m/D$, but this was primarily because the well-mixed locations were higher than the merging locations. The MAPE and NRMSE values are more useful for comparing the performance of the model in predicting $y_m/D$ and $y_w/D$. The NRMSE value can be defined as the RMSE value normalized by either the range or the mean of the experimental data, and the latter definition was employed in this study. The RMSE value for $y_w/D$ was

Table 2
Statistics and error analysis for the MGGP predictions

| Variable | MBE | MAE | MAPE (%) | RMSE | NRMSE (%) | $R^2$ |
|---|---|---|---|---|---|---|
| $y_m/D$ | 0.0066 | 0.0563 | 0.6474 | 0.0759 | 0.4083 | 1.0000 |
| $C_m/C_0$ | –0.0001 | 0.0016 | 0.5191 | 0.0024 | 0.5568 | 0.9999 |
| $y_w/D$ | 0.0660 | 0.4845 | 0.7191 | 0.7325 | 1.0800 | 0.9989 |
| $C_w/C_0$ | 0.0000 | 0.0007 | 1.1437 | 0.0011 | 1.2872 | 0.9997 |

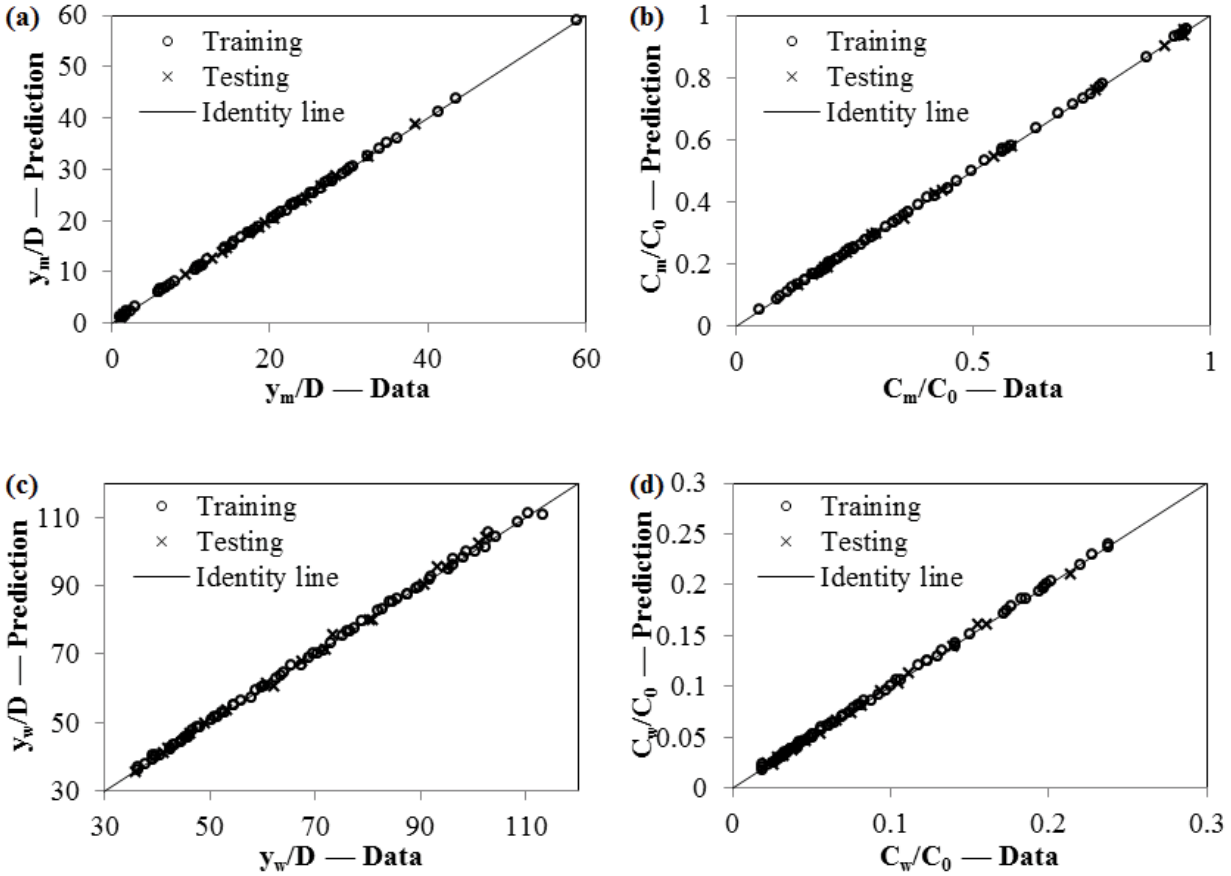


Fig. 5. Scatter plots of MGGP predictions of $y_m/D$, $C_m/C_0$, $Y_w/D$, and $C_w/C_0$.

0.7325, and the mean of the experimental data was 67.7924, and thus the NRMSE value was 1.0800%. The MAPE value was 0.7191%. Thus, the error in MGGP prediction for $y_w/D$ was about 0.9%, which was higher than that for $y_w/D$, indicating that the predictions obtained by the evolved model for $y_m/D$ were more reliable than those for $y_w/D$. The $R^2$ value was 0.9989, which was smaller than that for $y_m/D$, but this value was still very high, confirming the accuracy of the MGGP predictions for $y_w/D$.

For $C_w/C_0$, the absolute error indicators had very low values. The MBE value was almost zero because the biases for overestimation and under-estimation canceled out, indicating that the model accurately predicted the overall jet properties. The MAE and RMSE values were 0.0007 and 0.0011, respectively, so the error magnitude was about 0.001. This magnitude was smaller than that for $C_m/C_0$ primarily because the $C_w/C_0$ values were smaller than the $C_m/C_0$ values, as the jet was diluted along the upward trajectory. The MAPE and NRMSE values were 1.1437% and 1.2872%, respectively. Thus, the error in MGGP prediction for $C_w/C_0$ was about 1.2%, which was the only variable that had an error exceeding 1%. The $R^2$ value was 0.9997. The MAPE, NRMSE, and $R^2$ values implied that the evolutionary predictions for $C_w/C_0$ were less accurate than those for $C_m/C_0$; however, the errors were acceptably small, thus demonstrating that the evolved model can provide reasonable estimations.

### 3.3. Sensitivity analysis

A partial derivative sensitivity analysis (PDSA) [41,42] was conducted to evaluate how the varying inputs affected the $y_m/D$, $C_m/C_0$, $Y_w/D$, and $C_w/C_0$ for multiple vertical buoyant

jets in stationary ambient water. The sensitivity of the jet property parameter, $y_i$, to an input variable, $x_i$, was defined as the partial derivative $\partial y_i/\partial x_i$. The partial derivative at each point was calculated using Euler's numerical method, that is, $[y_i(x_i + \Delta h)\text{-}y_i(x)]/\Delta h$, where $\Delta h$ is a small step size, and the value of $y_i(x_i + \Delta h)$ was obtained by carrying out additional computations using the developed models.

The results of the sensitivity analysis for $y_m/D$ are presented in Fig. 6. The PDSA values in Fig. 6a were all positive, implying that $y_m/D$ increased with increased Sp. This was because the jets with greater port spacing needed to travel greater distances to arrive at the symmetry plane between two neighboring jets. Most of the PDSA values in Fig. 6b were negative, implying that $y_m/D$ generally decreased with increased Fr. A higher Fr number indicated a smaller density difference between the jet and ambient water, so the buoyancy effect, which forced the jet to move faster in the upward direction, became weaker as the Fr increased. Therefore, the upward velocity of the jet generally decreased in conjunction with increased Fr, which in turn caused $y_m/D$ to decrease. For the extreme case, with an Sp value of 10 and Fr value of 4.5, the jet merging occurred at a very high location, and small changes in Sp and Fr substantially affected the merging location. Except for this extreme case, the mean sensitivities of $y_m/D$ to Sp and Fr were 4.66 and –0.94 respectively, indicating that $y_m/D$ was more sensitive to Sp than to Fr. For the cases with large Fr values, the sensitivity of $y_m/D$ in relation to Fr was quite small, as shown in Fig. 6b, because the PDSA values approached zero.

Similarly, the results of the sensitivity analysis for $C_m/C_0$, $y_w/D$, and $C_w/C_0$ are presented in Fig. 7. The PDSA values for $C_m/C_0$ implied that $C_m/C_0$ decreased in conjunction with increased Sp; $C_m/C_0$ generally increased with increased Fr for small Fr values and decreased with increased Fr for the cases with large Fr values; $C_m/C_0$ was more sensitive to Fr. The PDSA values for $y_w/D$ implied that $y_w/D$ increased with increased Sp, and there was no clear trend for the sensitivity of $y_w/D$ in relation to Fr. The PDSA values for $C_w/C_0$ implied that $C_w/C_0$ decreased with increased Sp; $C_w/C_0$ generally increased in conjunction with increased Fr; $C_w/C_0$ was more sensitive to Sp than to Fr, and that the sensitivity became weaker with increasing values of Sp and Fr.

### 3.4. Uncertainty analysis

The uncertainty analysis results for the $y_m/D$, $C_m/C_0$, $y_w/D$, and $C_w/C_0$ models are presented in Table 3. The uncertainty analyses were conducted by using the MATLAB non-linear prediction confidence interval function "nlpredci". This function uses equations [43] based on the $t$ distribution, which gives a symmetric confidence interval at every point [44]. Further details regarding this function can be found in the literature [43–45]. The results in Table 3 indicate that the mean widths of the uncertainty bounds were ±0.473, ±0.013, ±4.621, and ±0.003 for $y_m/D$, $C_m/C_0$, $y_w/D$, and $C_w/C_0$.

### 3.5. Advantages and disadvantages of the models

A major contribution of the present study is that it demonstrated that the MGGP technique can be a promising tool for correlating the important characteristic variables of multiple jets with the flow input values, and that is provided explicit equations for calculating these characteristic variables. The results demonstrated the capability of the proposed models in accurately predicting $y_m/D$ (MAPE = 0.6474%; RMSE = 0.0759; $R^2$ = 1.0000), $C_m/C_0$ (MAPE = 0.5191%; RMSE = 0.0024;

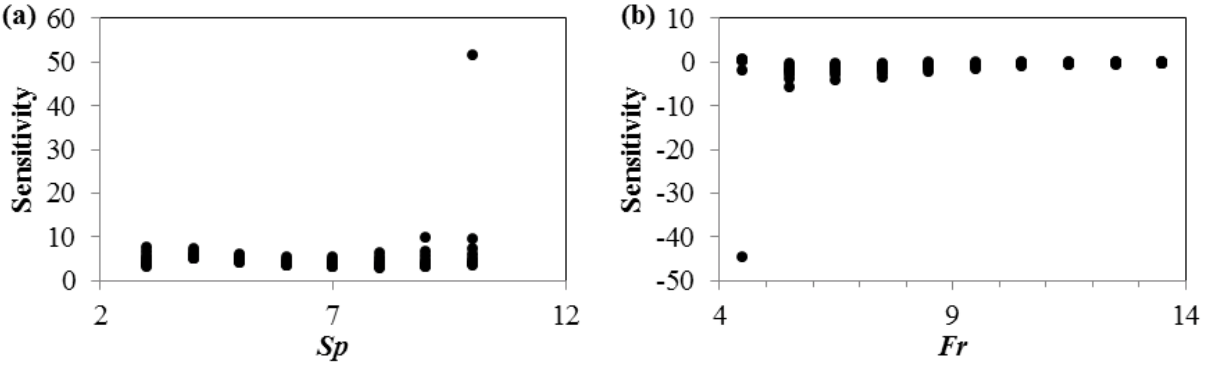


Fig. 6. Results of sensitivity analysis for $y_m/D$. (a) Sensitivity vs. Sp and (b) Sensitivity vs. Fr.

Table 3
Uncertainty analysis of the developed MGGP models

| Parameters | $y_m/D$ | $C_m/C_0$ | $y_w/D$ | $C_w/C_0$ |
|---|---|---|---|---|
| Mean uncertainty interval half-width | ±0.473 | ±0.013 | ±4.621 | ±0.003 |
| Mean 95% prediction error interval | (–0.466 0.479) | (–0.014 0.013) | (–4.555 4.687) | (–0.003 0.003) |
| Max uncertainty interval half-width | ±0.617 | ±0.016 | ±5.983 | ±0.004 |
| Max 95% prediction error interval | (–0.617 0.618) | (–0.016 0.017) | (–5.828 6.139) | (–0.003 0.005) |

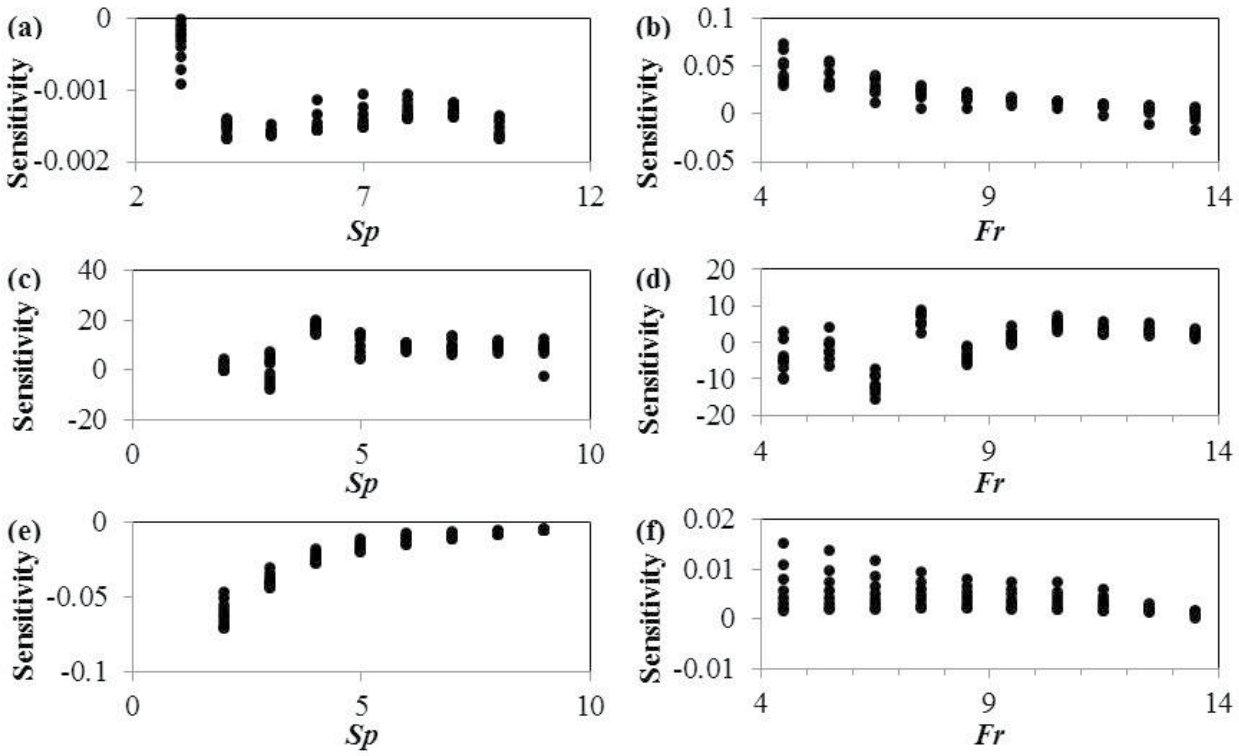


Fig. 7. Results of sensitivity analysis for $C_m/C_0$ (a and b), $y_w/D$ (c and d), and $C_w/C_0$ (e and f).

$R^2$ = 0.9999), $y_w/D$ (MAPE = 0.7191%; RMSE = 0.7325; $R^2$ = 0.9989), and $C_w/C_0$ (MAPE = 1.1437%; RMSE = 0.0011; $R^2$ = 0.9997). The observations from the sensitivity analyses were consistent with both the existing knowledge and engineering sense from the perspective of wastewater mixing engineering, confirming that the proposed models are capable of capturing the important mixing properties of multiple vertical buoyant jets in stationary ambient water.

It is acknowledged that the simulated data from the CFD model might already be representative of the average fitting function, and that one can simply run the validated CFD model for a specific configuration. However, developing MGGP models are still beneficial in two respects: first, a 3D CFD model typically takes days to complete one simulation, whereas an MGGP model can be run in seconds for a large number of cases and is thus much more efficient; second, an MGGP model can be continuously and readily improved or extended with the availability of more data. For uncomplicated problems, an empirical model based on traditional regression analysis may also be useful, but for multiple vertical buoyant jets, a generally accepted regression-based empirical model has not been reported because the mechanisms underlying the jet interactions are quite complicated.

A common drawback of a data-driven model, developed by either AI or traditional regression techniques, is that it is typically only valid within the range of the training data. Therefore, the present models are only reliable for the cases with Fr ranging from 4.5 to 13.5 and Sp ranging from 1 to 10. However, this is not a major concern because the training datasets already covered the typical data ranges for multiple vertical buoyant jets in practical applications, and an MGGP model can be continuously and readily improved upon and generalized with the availability of more data.

Another typical disadvantage of a model developed using that MGGP algorithm is that the physical significance in the mathematical expressions is not as clear as in physical-based or empirical models. This lack of clear physical significance in an MGGP model is partially due to two facts: first, MGGP detects hidden nonlinear relationships between variables, while physical-based or empirical models may only use a calibration or regression parameter to represent the relationships; second, MGGP uses linearly combined low-order nonlinear terms to describe a phenomenon, while physical-based models typically use complicated partial differential equations. Therefore, the sacrifice of obvious physical significance makes an MGGP model more accurate than an empirical model and much more efficient than a physical-based model, and the sacrifice is of less concern as long as the model is carefully tested.

## 4. Conclusions

The current paper has presented the application of the MGGP approach to developing a model for estimating the properties of multiple vertical buoyant jets in stationary ambient water. The focus has been on four characteristic parameters: the non-dimensional vertical displacement of the merging point ($y_m/D$), the non-dimensional centerline concentration ($C_m/C_0$) where the jets start merging, the non-dimensional vertical displacement of the well-mixed location ($y_w/D$), and the non-dimensional concentration where the jets are well mixed ($C_w/C_0$). The MGGP technique

was introduced in order to obtain explicit equations for these variables through an evolutionary process. The results demonstrated the capability of the proposed models in accurately predicting $y_m/D$, $C_m/C_0$, $y_w/D$, and $C_w/C_0$. Sensitivity analyses utilizing the PDSA approach were conducted to assess how varying the Sp and Fr values affect the characteristic variables, and the results revealed that $y_m/D$ and $C_w/C_0$ were more sensitive to Sp than to Fr, $C_m/C_0$ was more sensitive to Fr, and there was no clear trend regarding the sensitivity of $y_w/D$ in relation to Fr. Moreover, uncertainty analysis was conducted, and the uncertainty band-widths identified for $y_m/D$, $C_m/C_0$, $y_w/D$, and $C_w/C_0$ were ±0.473, ±0.013, ±4.621, and ±0.003, respectively. Therefore, the proposed MGGP models can be regarded as promising tools for studying jets discharged from multiport diffusers.

## Acknowledgments

This work was funded by the Natural Sciences and Engineering Research Council of Canada (NSERC Discovery Grants). One of the authors is a recipient of a scholarship from the China Scholarship Council (CSC).

## References

[1] O. Abessi, P.J. Roberts, Multiport diffusers for dense discharges, J. Hydraul. Eng., 140 (2014) 04014032.
[2] O. Abessi, P.J. Roberts, Multiport diffusers for dense discharge in flowing ambient water, J. Hydraul. Eng., 143 (2017) 04017003.
[3] S. Lyu, I.W. Seo, Y.D. Kim, Experimental investigation on behavior of multiple vertical buoyant jets discharged into a stagnant ambient, KSCE J. Civ. Eng., 17 (2013) 1820–1829.
[4] X. Tian, P.J. Roberts, Experiments on marine wastewater diffusers with multiport rosettes, J. Hydraul. Eng., 137 (2011) 1148–1159.
[5] X. Yan, A. Mohammadian, Numerical Modeling of Vertical Buoyant Jets Subjected to Lateral Confinement, J. Hydraul. Eng., 143 (2017) 04017016.
[6] T. Bleninger, G.H. Jirka, Modelling and environmentally sound management of brine discharges from desalination plants, Desalination, 221 (2008) 585–597.
[7] K.L. Pun, M.J. Davidson, H.J. Wang, Merging jets in a coflowing ambient fluid-a hybrid approach, J. Hydraul. Res., 38 (2000) 105–114.
[8] G.C. Christodoulou, I.G. Papakonstantis, I.K. Nikiforakis, Desalination brine disposal by means of negatively buoyant jets, Desal. Wat. Treat., 53 (2015) 3208–3213.
[9] G.C. Christodoulou, I.K. Nikiforakis, T.D. Diamantis, A.I. Stamou, Near-field dilution of a vertical dense jet impinging on a solid boundary, Desal. Wat. Treat., 57 (2016) 4898–4905.
[10] D. Drami, Y.Z. Yacobi, N. Stambler, N. Kress, Seawater quality and microbial communities at a desalination plant marine outfall. A field study at the Israeli Mediterranean coast, Water Res., 45 (2011) 5449–5462.
[11] S. Lattemann, T. Höpner, Environmental impact and impact assessment of seawater desalination, Desalination, 220 (2008) 1–15.
[12] I.K. Nikiforakis, A.I. Stamou, G.C, Christodoulou. Integrated modeling of single port brine discharges into unstratified stagnant ambient, Environ Fluid Mech., 17 (2017) 247–275.
[13] S. Zhang, B. Jiang, A.W.K. Law, B. Zhao, Large eddy simulations of 45 inclined dense jets, Environ Fluid Mech., 16 (2016) 101–121.
[14] A.M. Shinneeb, R. Balachandar, J.D. Bugg, Confinement effects in shallow-water jets, J. Hydraul. Eng., 137 (2010) 300–314.
[15] O. Abessi, M. Saeedi, M. Davidson, N.H. Zaker, Flow classification of negatively buoyant surface discharge in an ambient current, J. Coastal Res., 28 (2011) 148–155.
[16] C.J. Oliver, M.J. Davidson, R.I. Nokes, Removing the boundary influence on negatively buoyant jets, Environ Fluid Mech., 13 (2013) 625–648.
[17] B. Jiang, A.W.K. Law, J.H.W. Lee, Mixing of 30 and 45 inclined dense jets in shallow coastal waters, J. Hydraul. Eng., 140 (2013) 241–253.
[18] G.R. Jones, J.D. Nash, R.L. Doneker, G.H. Jirka, Buoyant surface discharges into water bodies. I: Flow classification and prediction methodology, J. Hydraul. Eng., 133 (2007) 1010–1020.
[19] I.K. Nikiforakis, A.I. Stamou, Integrated modelling for the discharge of brine from desalination plants into coastal waters, Desal. Wat. Treat., 53 (2015) 3214–3223.
[20] G.H. Jirka, Buoyant surface discharges into water bodies. II: Jet integral model, J. Hydraul. Eng., 133 (2007) 1021–1036.
[21] H. Gildeh, A. Mohammadian, I. Nistor, H. Qiblawey, Numerical modeling of turbulent buoyant wall jets in stationary ambient water, J. Hydraul. Eng., 140 (2014) 04014012.
[22] H. Gildeh, A. Mohammadian, I. Nistor, H. Qiblawey, X. Yan, CFD modeling and analysis of the behavior of 30° and 45° inclined dense jets–new numerical insights, J. Appl. Water Eng. Res., 4 (2015) 1–16.
[23] H. Gildeh, A. Mohammadian, I. Nistor, H. Qiblawey, Numerical modeling of 30° and 45° inclined dense turbulent jets in stationary ambient, Environ. Fluid Mech., 15 (2015) 537–562.
[24] A. Dashti, M. Asghari, H. Solymani, M. Rezakazemi, A. Akbari, Modeling of $CaCl_2$ removal by positively charged polysulfone-based nanofiltration membrane using artificial neural network and genetic programming, Desal. Wat. Treat., 111 (2018) 57–67.
[25] A.A. Tashvigh, B. Nasernejad, Soft computing method for modeling and optimization of air and water gap membrane distillation–a genetic programming approach, Desal. Wat. Treat., 76 (2017) 30–39.
[26] A.A. Tashvigh, F.Z. Ashtiani, M. Karimi, A. Okhovat, A novel approach for estimation of solvent activity in polymer solutions using genetic programming, Calphad, 51 (2015) 35–41.
[27] A.A. Tashvigh, F.Z. Ashtiani, A. Fouladitajar, Genetic programming for modeling and optimization of gas sparging assisted microfiltration of oil-in-water emulsion, Desal. Wat. Treat., 57 (2016) 19160–19170.
[28] A.H. Gandomi, A.H. Alavi, C. Ryan, Handbook of Genetic Programming Applications, Springer, Berlin, 2015.
[29] M.J.S. Safari, A.D. Mehr, Multigene genetic programming for sediment transport modeling in sewers for conditions of non-deposition with a bed deposit, Int. J. Sediment Res., 33 (2018) 262–270.
[30] D.P. Searson, In: A.H. Gandomi, Ed., Handbook of Genetic Programming Applications, Springer, Cham, 2015, pp. 551–573.
[31] A. Garg, A. Garg, K. Tai, S. Barontini, A. Stokes, A computational intelligence-based genetic programming approach for the simulation of soil water retention curves, Transport Porous Med., 103 (2014) 497–513.
[32] H. Kaydani, A. Mohebbi, M. Eftekhari, Permeability estimation in heterogeneous oil reservoirs by multi-gene genetic programming algorithm, J. Petrol Sci. Eng., 123 (2014) 201–206.
[33] A.D. Mehr, V. Nourani, Season algorithm-multigene genetic programming: a new approach for rainfall-runoff modelling, Water Resour. Manage., 32 (2018) 2665–2679.
[34] X. Yan, A. Mohammadian, Multigene Genetic-Programming-Based Models for Initial Dilution of Laterally Confined Vertical Buoyant Jets, J. Marine Sci. Eng., 7 (2019) 246.
[35] X. Yan, A. Mohammadian, Evolutionary modeling of inclined dense jets discharged from multiport diffusers, J. Coastal Res., 2019, https://doi.org/10.2112/JCOASTRES-D-19-00057.1
[36] A.B. Pincince, E.J. List, Disposal of brine into an estuary, J Water Pollut. Control Fed., 45 (1973) 2335–2344.
[37] P.J. Roberts, G. Toms, Inclined dense jets in flowing current, J. Hydraul. Eng., 113 (1987) 323–340.
[38] N.G. Jacobsen, D.R. Fuhrman, J. Fredsøe, A wave generation toolbox for the open-source CFD library: OpenFoam®, Int. J. Numer. Methods Fluids, 70 (2012) 1073–1088.
[39] F. Farshi, A. Kabiri-Samani, M.R. Chamani, H. Atoof, Evaluation of the secondary current parameter and depth-averaged

velocity in curved compound open channels, J. Hydraul. Eng., 144 (2018) 04018059.
[40] H. Bashiri, E. Sharifi, V.P. Singh, Prediction of local scour depth downstream of sluice gates using harmony search algorithm and artificial neural networks, J. Irrig. Drain. Eng., 144 (2018) 06018002.
[41] H. Azimi, H. Bonakdari, I. Ebtehaj, A highly efficient gene expression programming model for predicting the discharge coefficient in a side weir along a trapezoidal canal, Irrig. Drain., 66 (2017) 655–666.
[42] I. Ebtehaj, H. Bonakdari, A.H. Zaji, H. Azimi, F. Khoshbin, GMDH-type neural network approach for modeling the discharge coefficient of rectangular sharp-crested side weirs, Eng. Sci. Technol. Int. J., 18 (2015) 746–757.
[43] G.A.F. Seber, C.J. Wild, Nonlinear Regression, John Wiley & Sons, New York, 1989.
[44] K.D. Dolan, L. Yang, C.P. Trampel, Nonlinear regression technique to estimate kinetic parameters and confidence intervals in unsteady-state conduction-heated foods, J. Food Eng., 80 (2007) 581–593.
[45] T.P. Lane, W.H. DuMouchel, Simultaneous confidence intervals in multiple regression, Am. Stat., 48 (1994) 315–321.